

Center vortex model for the infrared sector of $SU(4)$ Yang-Mills theory: String tensions and deconfinement transition

M. Engelhardt¹

*Physics Department, New Mexico State University
Las Cruces, NM 88003, USA*

Abstract

A random vortex world-surface model for the infrared sector of $SU(4)$ Yang-Mills theory is constructed, focusing on the confinement properties and the behavior at the deconfinement phase transition. Although the corresponding data from lattice Yang-Mills theory can be reproduced, the model requires a more complex action and considerably more tuning than the $SU(2)$ and $SU(3)$ cases studied previously. Its predictive capabilities are accordingly reduced. This behavior has a definite physical origin, which is elucidated in detail in the present work. As the number of colors is raised in Yang-Mills theory, the corresponding infrared effective vortex description cannot indefinitely continue to rely on dynamics determined purely by vortex world-surface characteristics; additional color structures present on the vortices begin to play a role. As evidenced by the modeling effort reported here, definite signatures of this behavior appear in the case of four colors.

PACS: 12.38.Aw, 12.38.Mh, 12.40.-y

Keywords: Center vortices, infrared effective theory, confinement

¹email: engel@nmsu.edu

1 Introduction

The vortex picture of the strong interaction vacuum was originally conceived [1–5] as an explanation for confinement. More recent work [6–23] has established it as a comprehensive, and in many respects quantitative infrared effective model of the vacuum, generating not only confinement, but also the spontaneous breaking of chiral symmetry and the axial $U_A(1)$ anomaly. The evidence for the vortex picture rests on two pillars. On the one hand, methods have been developed which permit the identification and isolation of vortex structures in the gauge configurations of lattice QCD [6, 7, 19]. Based on these techniques, the phenomenology induced by the vortices present in lattice gauge configurations can be studied. Highlights of the results obtained in this manner include vortex dominance of the string tension [6, 7, 19], the absence of nonperturbative effects (string tension, chiral condensate, topological susceptibility) when vortices are removed from lattice gauge configurations [18, 19], and a natural explanation of the deconfining phase transition as a vortex percolation transition [16].

On the other hand, an infrared effective random vortex world-surface model has been developed [21–27] which demonstrates that the main nonperturbative features of the strong interaction vacuum can be described² on the basis of a *weakly coupled* vortex dynamics. This further buttresses the notion that vortices constitute the relevant infrared gluonic degrees of freedom in that vacuum. Through its reduced set of degrees of freedom and the correspondingly simplified dynamics, the random vortex world-surface model has allowed the investigation of a wider range of scenarios than has been accessible using the vortices extracted from lattice gauge configurations discussed further above. In the random vortex world-surface model, not only has the $SU(2)$ case been investigated comprehensively [21–23], but also the confining properties of the $SU(3)$ case have been studied in detail [24–26], and the present work extends the model to $SU(4)$ color.

2 Motivation

2.1 Vortex color structure

To clarify the motivation for the present investigation, it is useful to begin by reviewing the different color structures which can occur on center vortices, specifically in various Abelian formulations. As will be discussed below, vortices are not only characterized by their location in space-time, but possess considerable additional structure in color space. In general, it cannot be excluded that this structure may significantly influence vortex dynamics; besides geometrical world-surface characteristics, the vortex effective

²In the $SU(2)$ and $SU(3)$ models studied to date, adjustment of a single dimensionless coupling constant suffices to arrive at a phenomenologically viable model, a number of nonperturbative observables being quantitatively predicted as a result. The $SU(4)$ case investigated here turns out to behave less favorably in this respect, and the reasons behind this represent a principal focus of the present work.

action potentially may also include a dependence on the aforementioned color structure. Investigation of the possibility or even necessity of such a dependence is a principal focus of the present investigation. Thus, a review of vortex color structure is in order.

Center vortices are closed tubes of quantized chromomagnetic flux in three spatial dimensions. Accordingly, they are described by (thickened) world-surfaces in four-dimensional (Euclidean) space-time. The quantization is defined by the property that a Wilson loop encircling a vortex (more precisely, linked to the latter) acquires a factor corresponding to a center element of the gauge group. In $SU(N)$ gauge theory, there are thus $N - 1$ possible vortex fluxes (the trivial unit element corresponds to no flux being present). In particular, this entails that vortices can branch for $N \geq 3$, as described in greater detail below.

This description of vortices in terms of their space-time location and their influence on Wilson loops is in some respects incomplete. While it is adequate for the discussion of the confinement properties encoded in Wilson loops, to fully describe the topological properties of vortices and the related chiral symmetry breaking phenomena, it is necessary to take into account the direction of the vortex field strength in color space [12–14, 22, 23, 28, 29]. While this direction can be rotated by gauge transformations, certain properties of it carry gauge-independent significance. For instance, generic vortex world-surfaces are nonorientable; this implies that the field strength cannot be globally proportional to a constant color vector. Instead, the color direction of the field strength must vary, in any gauge. While the detailed local space-time form of the variation forced by vortex nonorientability is gauge-dependent, it contains invariant characteristics which manifest themselves, e.g., in the topological charge.

Often, it is convenient to construct vortex configurations in an Abelian gauge. In this case, variations of the field strength color vector are compressed into lines on the vortex world-surfaces, leaving the color vector constant elsewhere. At these lines, the field strength is discontinuous in a way which corresponds to the presence of a source or sink of magnetic flux, i.e., an Abelian magnetic monopole. Thus, due to the nonorientability of vortex world-surfaces, monopoles represent an intrinsic feature of vortex configurations in Abelian gauges.

From this more detailed perspective, in particular also the branching points (in three-dimensional space) or lines (in four-dimensional space-time) of vortices mentioned further above can be characterized more thoroughly. Vortex branchings in general are associated with nontrivial rearrangements in the vortex color structure; they cannot be realized while keeping all vortex field strengths in the branching region pointing into the same fixed color direction, as will be discussed below.

To facilitate this discussion, (Abelian) vortex color direction will be specified in the following by giving the (diagonal) chromomagnetic flux matrix Q which results when evaluating a closed line integral encircling the vortex,

$$Q = \oint dx_\mu A_\mu . \tag{1}$$

This eliminates the detailed space-time information on the vortex field strength which is non-essential to the following discussion. In terms of Q , the Wilson loop along the same path is

$$W = \frac{1}{N} \text{Tr} \exp(iQ) . \quad (2)$$

Note that every vortex world-surface can be associated with two possible orientations, which yield opposite signs for Q . Conversely, of course, inverting the integration direction in the line integral defining Q inverts the sign of the latter. In order to preserve rotational symmetry in the following, if a given description allows for vortices associated with the color matrix Q , it will also include those associated with the color matrix $-Q$.

2.2 Minimal Abelian construction

The color structure of vortex branchings can now be viewed in a variety of ways. One possible picture results if one chooses a minimal set of definite (Cartan) color directions to describe the $N - 1$ types of vortex flux permitted by the gauge group. Under this very restrictive condition, vortex branching is tied to the presence of magnetic monopoles. Consider the $SU(3)$ gauge group as an example. The two nontrivial center elements are

$$\exp(2\pi i/3) , \quad \exp(-2\pi i/3) . \quad (3)$$

These are the phases which can arise in a Wilson loop due to linking with vortices. Since these two phases are complex conjugates of one another, they can actually be generated by the two possible orientations of one single type of vortex. Consequently, if one insists on using a minimal set of color directions, only one color matrix Q , along with its negative $-Q$, is necessary to construct all possible vortex configurations. Without loss of generality, let

$$Q = \frac{2\pi}{3} \text{diag}(1, 1, -2) . \quad (4)$$

Now, consider a vortex branching. The only way to divide an incoming vortex flux Q into two outgoing fluxes is by letting the latter each be associated with the flux $-Q$. Otherwise, evaluating Wilson loops encircling the incoming vortex or both the outgoing vortices, respectively, would yield different results, violating the Bianchi constraint (continuity of flux modulo 2π). However, even in the allowed branching configuration, the incoming flux is not simply the sum of the outgoing fluxes; the flux matrix is discontinuous. There is a sink of flux $3Q$ at the branching (which is compatible with the Bianchi constraint); this is an Abelian magnetic monopole³.

³Note furthermore that, in this particular case, branchings are the *only* locations where monopoles can be present. A switch from a flux Q to a flux $-Q$ along a single vortex does not correspond to a monopole allowed by the Bianchi constraint. This is different from the $SU(2)$ case, where a switch from $Q_{SU(2)} = \pi \text{diag}(1, -1)$ to $-Q_{SU(2)}$ is possible. In the minimal description of $SU(3)$ vortices, therefore, the vortex branching and the Abelian monopole concepts can be used synonymously. Note that this strict identification does not persist for $SU(4)$; in that case, monopoles can be present away from branchings even in the minimal description.

As a consequence, one can also take an alternative stance. Instead of discussing branchings for $N \geq 3$ in particular, and noting that monopoles are present at branchings, one can take the point of view that vortex configurations in general contain monopoles, which are sources or sinks of up to N vortex fluxes. Monopoles are connected by vortices, and between monopoles, vortex fluxes are oriented. Note that, in this language, there is no conceptual distinction between the cases $N = 2$ and $N \geq 3$. Both cases are described in the same language. In the former case, only two vortices emanate from any monopole, whereas for higher N , there can be two or more vortices emanating from monopoles, cf. also Fig. 1 below. This subsumes the statement that vortices branch for $N \geq 3$, while maintaining the same conceptual framework for all N .

2.3 Nexus construction

Alternative ways to describe the color structure of vortex branchings result if one allows for a non-minimal set of color flux matrices. In particular, if one uses a sufficiently large set of different flux matrices Q along with their negatives $-Q$, one can completely disassociate Abelian monopoles from branchings. Such a description of branchings was introduced in [12–14] along with the term “nexus” to refer to these objects⁴. Staying with the $SU(3)$ example, the relevant flux matrices are

$$\frac{2\pi}{3} \text{diag}(1, 1, -2), \quad \frac{2\pi}{3} \text{diag}(1, -2, 1), \quad \frac{2\pi}{3} \text{diag}(-2, 1, 1) \quad (5)$$

(along with their negatives). By letting each of the three vortices meeting at a branching be associated with a different flux matrix, monopoles can be completely avoided at branchings⁵. Of course, the global structure of the vortex world-surfaces will in general force monopoles to be present elsewhere (which is consistent with the nexus description, in contradistinction to the minimal description discussed above).

On the other hand, note that the nexus language distinguishes the $N = 2$ and the $N \geq 3$ cases on a qualitative level. The former case does not allow for (quasi-Abelian) nexi, i.e., branchings, whereas all other cases do [12].

2.4 Dynamical issues

Whether one views vortex color structure in terms of Abelian monopoles alone (as discussed at the end of section 2.2) or chooses to differentiate between nexi (i.e., branchings)

⁴More precisely, these are referred to as “quasi-Abelian” nexi in [12–14]. On the other hand, the “fully non-Abelian” nexi of [12–14] correspond, after a (singular) gauge transformation, to the “Abelian monopoles” of the present work.

⁵This property is likely to single out the quasi-Abelian nexus construction of branchings as the one most suited in practice for the purpose of evaluating the topological charge of general $SU(3)$ vortex world-surface configurations; this is currently under investigation.

and monopoles, these objects embody a nontrivial color structure which suggests an alternative characterization of the Yang-Mills vortex vacuum. Instead of viewing vortex world-surfaces as the only dynamical degrees of freedom, which happen to force the presence of certain color structures through their geometrical properties (nonorientability, branching), one can alternatively view monopoles (and nexi) as bona fide degrees of freedom, which, at least to a certain extent, determine the form of the vortex fluxes emanating from them and connecting them. Which of these pictures is the more appropriate one is a dynamical question; phrased more formally, is the vortex effective action dominated by terms involving geometrical vortex world-surface characteristics or by terms involving monopole (and nexus) characteristics?

In the $SU(2)$ and $SU(3)$ cases studied to date, effective vortex actions based purely on world-surface characteristics appear entirely adequate to reproduce the infrared sectors of the respective Yang-Mills theories on a quantitative level. Specifically, vortices are controlled by world-surface curvature in the $SU(2)$ and $SU(3)$ models. However, it would be rather surprising if this picture persisted indefinitely as the number of colors N is increased; on the contrary, a shift towards dynamics influenced by monopole (or nexus) characteristics is likely, as has been argued previously [30]. This is expected because, as the number of colors rises, center flux can be quantized in ever smaller units, while the monopoles always constitute sources or sinks of flux 2π , or multiples thereof (in each diagonal color component), cf. Fig. 1. Thus, it seems plausible that monopoles become the dominant carriers of inertia in vortex configurations, and that the vortex world-surfaces then adjust to the monopole positions rather than the latter being determined by the world-surface dynamics. This should manifest itself in an effective vortex action in which the monopoles (or nexi) attain their own dynamical significance.



Figure 1: Vortex configurations contain monopoles, cf. section 2.2. For N colors, up to N vortex fluxes can emanate from any given monopole. Examples for $N = 2$ (left) and $N = 8$ (right) are depicted. In order to display a generic case, for $N = 8$ also a vortex associated with center phase $e^{iQ} = e^{i\pi/2}$ (the double line) has been included (all the other vortices carry center phase $e^{iQ} = e^{i\pi/4}$). As N rises, center flux can be quantized in ever smaller units, while monopoles remain sources or sinks of flux 2π , or multiples thereof (in each diagonal color component).

To search for indications of this shift in the dynamical characteristics, and thus probe the limits of applicability of pure random world-surface dynamics for center vortices, was the principal motivation for the present $SU(4)$ work. Indeed, of the effective vortex

actions investigated below, only ones including an explicit dependence on branching properties prove to be phenomenologically viable. Before proceeding to describe the investigation in detail, it should be emphasized that the possibility of such a shift in the dynamical characteristics does not imply that the vortex picture as a whole may become inappropriate at larger N and that, e.g., an Abelian monopole Coulomb gas may become an appropriate description. On the contrary, for any finite N , chromomagnetic flux must be constricted into center vortices in order to, e.g., correctly account for the lack of confinement of adjoint color sources [8]. The aforementioned shift in the characterization of the vacuum merely concerns the specific form of the effective vortex action; vortices nonetheless continue to represent relevant infrared degrees of freedom. All that is implied is that, at larger N , the Abelian monopoles which intrinsically reside on generic non-orientable vortex world-surfaces (in Abelian gauges) may cease to be completely dependent objects with no dynamical significance of their own; instead, their characteristics may begin to play a role in determining overall vortex configuration dynamics⁶.

3 SU(4) vortex model

3.1 Degrees of freedom

Vortex flux quantization in the $SU(4)$ vortex model is determined by the three nontrivial center elements i , $-i$ and -1 of the $SU(4)$ gauge group. The former two elements are complex conjugates of one another and thus can be generated by the two possible orientations of one type of vortex. Therefore, the $SU(4)$ model contains in all two physically different types of vortices; the ones generating a phase -1 and the ones generating the phases $\pm i$ depending on their orientation in space-time.

The $SU(4)$ random vortex world-surface model is constructed in complete analogy to the $SU(2)$ and $SU(3)$ cases studied previously. The reader is referred to [21, 24] for details regarding the physical interpretation of the construction. The vortex world-surfaces are modeled by composing them of elementary squares on a hypercubic lattice. Each elementary square in the lattice is associated with a value

$$q_{\mu\nu}(x) \in \{-1, 0, 1, 2\}, \quad q_{\nu\mu}(x) = -q_{\mu\nu}(x) \quad (6)$$

where the square extends from the point x into the positive μ and ν directions. The right-hand relation is simply a reminder of the behavior of flux under space-time inversions, i.e., when the orientation of the vortex surface is reversed. In practice, recording only $q_{\mu\nu}(x)$ for $\mu < \nu$ is sufficient. The value $q_{\mu\nu}(x) = 0$ corresponds to no vortex flux being present on the square in question; nonzero values of $q_{\mu\nu}(x)$ could, e.g., label the first

⁶Merely at infinite N , where the center of the $SU(N \rightarrow \infty)$ gauge group becomes $Z(N \rightarrow \infty) \simeq U(1)$, a pure monopole description may be feasible. There, center quantization of flux ceases to constitute a constraint, since arbitrarily small units of center flux are possible.

element of the flux matrix $Q_{\mu\nu}(x)$ associated with the elementary square in a minimal Abelian construction,

$$Q_{\mu\nu}(x) \in \left\{ \frac{\pi}{2} \text{diag}(-1, -1, -1, 3), \frac{\pi}{2} \text{diag}(1, 1, 1, -3), \frac{\pi}{2} \text{diag}(2, 2, -2, -2) \right\} \quad (7)$$

(since, in the following, only Wilson loops and action densities will be studied, it is not necessary to distinguish between the last flux matrix in (7) and the one corresponding to inverse orientation; for a study, e.g., of topological properties, this would be necessary).

An important point to be noted is that the lattice spacing in this approach is a fixed physical quantity implementing the notion that vortices possess a finite transverse thickness and must be a minimal distance apart to be distinguished from one another⁷. This is discussed in detail in [21, 24]. While in the $SU(2)$ and $SU(3)$ models, there is only one type of center vortex (up to orientation), in the present $SU(4)$ case, there are two physically distinct types of vortices. In general, these can have different thicknesses. However, there is no straightforward way of implementing variable thicknesses in the present hypercubic lattice formulation of the model; all vortices will be described using a single lattice. This model restriction should be kept in mind.

Ensembles of random vortex world-surface configurations on lattices are generated using Monte Carlo methods. The elementary update of a given vortex surface configuration can be effected such that the Bianchi constraint is respected at every step. This is achieved by updating all six faces of an elementary three-dimensional cube in the lattice at once, in a way which corresponds to adding a vortex flux of the shape of the cube surface to the flux previously present. Formally, if the elementary cube in question extends from the lattice site x into the positive μ , ν and λ directions, then update simultaneously

$$\begin{aligned} q_{\mu\nu}(x) &\rightarrow (q_{\mu\nu}(x) + w) \bmod 4, & q_{\mu\nu}(x + e_\lambda) &\rightarrow (q_{\mu\nu}(x + e_\lambda) - w) \bmod 4 \\ q_{\nu\lambda}(x) &\rightarrow (q_{\nu\lambda}(x) + w) \bmod 4, & q_{\nu\lambda}(x + e_\mu) &\rightarrow (q_{\nu\lambda}(x + e_\mu) - w) \bmod 4 \\ q_{\lambda\mu}(x) &\rightarrow (q_{\lambda\mu}(x) + w) \bmod 4, & q_{\lambda\mu}(x + e_\nu) &\rightarrow (q_{\lambda\mu}(x + e_\nu) - w) \bmod 4 \end{aligned} \quad (8)$$

where the value $w \in \{-1, 1, 2\}$ characterizing the superimposed flux in practice is chosen at random with equal probability, and the modulo operation is to be carried out such that the result again satisfies $q \in \{-1, 0, 1, 2\}$. Since the update effects a linear superposition of two fluxes which satisfy the Bianchi constraint, the updated configuration again satisfies that constraint (the modulo operation merely generates shifts by 2π in the flux matrix, which are allowed by the Bianchi constraint; in this way, monopoles appear in the vortex configuration as the updates proceed).

⁷In the $SU(2)$ and $SU(3)$ models, the lattice spacing turns out to be 0.39 fm if one fixes the scale by setting the zero-temperature string tension to $\sigma(T=0) = (440 \text{ MeV})^2$.

3.2 Action

Finally, the action weighting vortex world-surface configurations must be specified. The most general form of the action used is the sum

$$S[q] = S_{\text{curv}}[q] + S_{\text{area}}[q] + S_{\text{branch}}[q] \quad (9)$$

with the individual terms specified as follows.

The immediate generalization of the dynamics studied in the $SU(2)$ and $SU(3)$ models is a world-surface curvature action, adapted to the present case, in which there are two physically distinct types of vortices,

$$S_{\text{curv}}[q] = \sum_x \sum_\mu \left[\sum_{\substack{\nu < \lambda \\ \nu \neq \mu, \lambda \neq \mu}} \left(C(|q_{\mu\nu}(x) q_{\mu\lambda}(x)|) + C(|q_{\mu\nu}(x) q_{\mu\lambda}(x - e_\lambda)|) \right. \right. \\ \left. \left. + C(|q_{\mu\nu}(x - e_\nu) q_{\mu\lambda}(x)|) + C(|q_{\mu\nu}(x - e_\nu) q_{\mu\lambda}(x - e_\lambda)|) \right) \right] \quad (10)$$

with

$$C(0) = 0 \quad C(1) = c_{11} \quad C(2) = c_{12} \quad C(4) = c_{22} . \quad (11)$$

Note that this action term (as well as all others below) treats $q = \pm 1$ fluxes symmetrically, as it should, since these two cases correspond to the two possible orientations of the same physical vortex type. As is clear from the expression given, for each link extending from the site x into the positive μ direction, all pairs of elementary squares attached to that link are examined, excluding those in which the two squares lie in the same plane. Depending on the flux associated with the squares, an action increment is incurred. Thus, world-surfaces are penalized for going around a corner, i.e., for curvature. In the following, the couplings c_{ij} will be generated from two independent coefficients c_1, c_2 (corresponding to the two physically distinct types of vortices) as

$$c_{ij} = c_i c_j . \quad (12)$$

Note that giving c_{12} special treatment, i.e., generalizing to $c_{12} \neq c_1 c_2$, to an extent would amount to a special treatment of branchings (along with related features such as different vortex types intersecting along a whole line), since branchings are locations where a $q = 2$ vortex splits into two $q = \pm 1$ vortices. However, on the other hand, an additional action term weighting branchings *explicitly* will be introduced separately below. For this reason, the option $c_{12} \neq c_1 c_2$ was not pursued further in this investigation (even though, strictly speaking, it is physically distinct from the aforementioned branching action). Instead, the explicit branching action term introduced below will be studied extensively.

A further type of action investigated in the $SU(2)$ and $SU(3)$ models is an action simply weighting world-surface area,

$$S_{\text{area}}[q] = \sum_x \sum_{\mu < \nu} A(|q_{\mu\nu}(x)|) . \quad (13)$$

In the $SU(2)$ and $SU(3)$ models, it was found that this action term could be traded off against the curvature term, and it was therefore ultimately discarded. Essentially, in the random surface ensemble, total surface area is strongly correlated with total curvature content, such that, for all practical purposes, the area term can be replaced by a strengthening of the curvature term for a wide range of parameters [21,24]. In the present work, the effects of this term are briefly explored, cf. section 5.2 below; inclusion of this term however does not appear to increase the phenomenological flexibility of the model.

Finally, a new term introduced in the present investigation is an explicit weighting of branchings,

$$S_{\text{branch}}[q] = \sum_x \sum_\mu B \left(\sum_{\nu \neq \mu} E(q_{\mu\nu}(x)) + E(q_{\mu\nu}(x - e_\nu)) \right) \quad (14)$$

where

$$E(0) = 0, \quad E = 1 \text{ else} \quad (15)$$

$$B(3) = B(5) = -b, \quad B = 0 \text{ else} \quad (16)$$

This action term precisely encourages vortex branchings: For each link extending from the site x into the positive μ direction, the number of attached elementary squares occupied by vortex flux is counted and, if that number equals 3 or 5 (which happens precisely when branching takes place), the action is decremented by the branching coefficient b . Further below, it will be shown why the introduction of this type of term is necessary to arrive at a phenomenologically viable model, corroborating the general arguments of section 2. In view of the different vortex formulations discussed in section 2, one can interpret S_{branch} as favoring the presence of nexi, or alternatively as favoring the presence of (certain types of) Abelian monopoles. Whichever picture one may choose, the introduction of this term represents a departure from pure vortex world-surface dynamics, according additional color structures present on the vortex world-surfaces their own dynamical significance.

4 $SU(4)$ Yang-Mills lattice data

The $SU(4)$ lattice data which will be matched in the random vortex world-surface model are drawn from [31,32]. After the bulk of the numerical work in the present investigation was completed, updated lattice data became available [33]. The author did not attempt to adjust the vortex model to the revised data, since the quantitative adjustments this would entail do not alter the conclusions drawn.

On the other hand, [33] also contains lattice data on the spatial string tension, for which no measurements were available previously. These data will be compared to corresponding predictions within the vortex model constructed here in section 5.3.

Specifically, the $SU(4)$ Yang-Mills characteristics which will be matched in the vortex model are the following:

4.1 String tension and deconfinement temperature

The ratio of the deconfinement temperature T_c to the zero-temperature quark string tension σ_1 is taken to be [31]

$$\frac{T_c}{\sqrt{\sigma_1}} = 0.62 . \quad (17)$$

The quantity $T_c/\sqrt{\sigma}$ was also used in the $SU(2)$ and $SU(3)$ models to fix the single curvature coefficient c ; since that curvature coefficient represented the only (physically significant) adjustable parameter, no further lattice data were needed to fully define those models.

4.2 String tension ratios

In correspondence to the two different types of center vortices present in the $SU(4)$ theory, there are also two distinct string tensions, the quark string tension σ_1 and the diquark string tension σ_2 . Data on both is needed to fix the two curvature coefficients c_1, c_2 of the $SU(4)$ vortex model. Thus, as one generalizes the vortex model to a higher number of colors, it does not generally predict ratios between different string tensions, unless one makes further prior assumptions about relationships between the properties of different types of vortices; for such considerations at large N , cf. [30]. Rather, the vortex model always provides sufficient freedom to match all relevant string tension ratios, since there are correspondingly many physically distinct types of vortices with their separate dynamical characteristics such as curvature coefficients, etc.

The ratio of the diquark string tension to the quark string tension at zero temperature is taken to be [32]

$$\frac{\sigma_2}{\sigma_1} = 1.36 . \quad (18)$$

4.3 First order character of the deconfinement transition

The first-order character of the deconfinement phase transition becomes more pronounced as one raises the number of colors. In units of T_c^4 , the latent heat of $SU(4)$ Yang-Mills theory is larger than the one of $SU(3)$ Yang-Mills theory by a factor of 2.25 [31]. As will be described below, the $SU(4)$ vortex model with a pure curvature action (10) does not reproduce this property, even on a qualitative level. This is the reason for the introduction of the new branching action (14); a more detailed motivation for that particular choice follows further below. Introducing this additional action term introduces the new branching coefficient b ; to fix this coefficient, an additional piece of

lattice data is needed. The aforementioned relation between latent heats in the $SU(3)$ and $SU(4)$ cases can be restated as

$$\Delta s \frac{T_c^4}{\sigma_1^4} \Big|_{SU(4)} = 2 \cdot \Delta s \frac{T_c^4}{\sigma^4} \Big|_{SU(3)} \quad (19)$$

using (17) as well as the relation $T_c/\sqrt{\sigma} = 0.63$ for $SU(3)$ used in [24], where Δs denotes the difference in action density (per space-time volume) between the two coexisting phases at the deconfinement temperature. This modified choice of units was adopted because it has more moderate scaling properties as one investigates the vortex model on lattices of different (Euclidean) temporal extent N_t , cf. below.

In order to be able to model the property (19), it is necessary to briefly revisit the $SU(3)$ vortex model [24]. The case of lattices with an extension of $N_t = 2$ lattice spacings in the Euclidean time direction is discussed in detail in [24]; the deconfinement transition is found at the value $c = 0.2359$ for the curvature coefficient. Reading off the discontinuity in the action density at the phase transition from the corresponding action density distribution⁸, one has (with a denoting the lattice spacing)

$$\Delta s = 0.45 T_c^4 \quad (T_c a = 1/2, \quad c = 0.2359, \quad \sigma a^2 = 0.695) \quad (20)$$

where the value for the zero-temperature string tension σ measured separately for $c = 0.2359$ has been included for later reference. The physical point of the $SU(3)$ model is not at $c = 0.2359$, but nearby at $c = 0.21$. This can be corrected for by also considering $N_t = 1$ and interpolating in c . For $N_t = 1$, the deconfinement transition is found for $c = 0.0872$. Producing an action density distribution analogous to the one discussed above for $N_t = 2$ permits one to read off

$$\Delta s = 0.022 T_c^4 \quad (T_c a = 1, \quad c = 0.0872, \quad \sigma a^2 = 1.355) . \quad (21)$$

The zero-temperature string tension σ was again measured separately for this value of c . From (20) and (21), the strong variation of Δs as a function of c in the units given is evident. As a consequence, these units are not well suited for interpolation in c , and it is indeed advantageous to convert to

$$\Delta s \frac{T_c^4}{\sigma^4} \Big|_{c=0.2359} = 0.0075 , \quad \Delta s \frac{T_c^4}{\sigma^4} \Big|_{c=0.0872} = 0.0065 . \quad (22)$$

⁸Note that the distributions in [24] are plotted as a function of the action per link divided by the curvature coefficient c ; therefore, to obtain Δs , one needs to multiply by $4c/a^4$, where a denotes the lattice spacing. Note also that the rough measure for the action density discontinuity used here and throughout this work is simply the distance between the two maxima in the action density distribution plot (instead of, e.g., modeling the latter as a superposition of two distributions). Since only ratios between discontinuities are of interest here, the effects of this slight underestimate cancel to a sufficient degree for the present purposes.

Finally, interpolating linearly to the physical point $c = 0.21$, one has

$$\Delta s \frac{T_c^4}{\sigma^4} \Big|_{SU(3)} = 0.0074 \quad (23)$$

and, inserting into (19), the condition to be satisfied by the $SU(4)$ model is therefore

$$\Delta s \frac{T_c^4}{\sigma_1^4} \Big|_{SU(4)} = 0.015 . \quad (24)$$

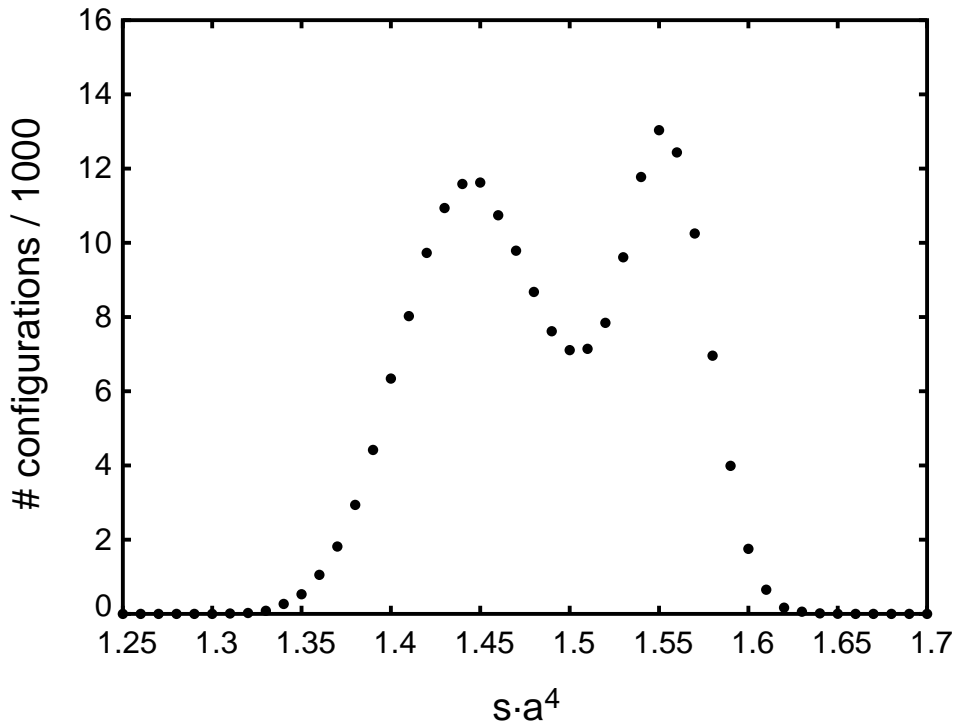


Figure 2: Distribution of the action density s (per space-time volume) at the deconfining phase transition, for a pure vortex world-surface curvature action with $c_1 = c_2 = 0.4722$. The measurement was taken on a $14^3 \times 2$ lattice; a denotes the lattice spacing.

5 Exploration of coupling parameter space

5.1 Pure world-surface curvature action

As a starting point, consider the $SU(4)$ random vortex world-surface model with a pure curvature action (10),(12), restricted to equal curvature coefficients, $c_1 = c_2$. This is

not yet very realistic as far as the condition (18) is concerned; for $c_1 = c_2$, one obtains $\sigma_1 = \sigma_2$, i.e., $\sigma_2/\sigma_1 = 1$. On the other hand, one does observe a deconfinement transition which is quite strongly first order, cf. Fig. 2 for $N_t = 2$, taken at $c_1 = c_2 = 0.4722$. Similar observations can be made at other N_t , with corresponding $c_1 = c_2$; the case $N_t = 2$ is the one which comes closest to satisfying the remaining condition (17). Note that the physical set of parameters in the random vortex world-surface model is generally such that the inverse deconfinement temperature is not an integer multiple of the lattice spacing; properties of the deconfinement transition at the physical point then cannot be measured directly, but are inferred by interpolation of data obtained at different N_t , cf. the treatment of the $SU(3)$ case above and cf. also [21, 24].

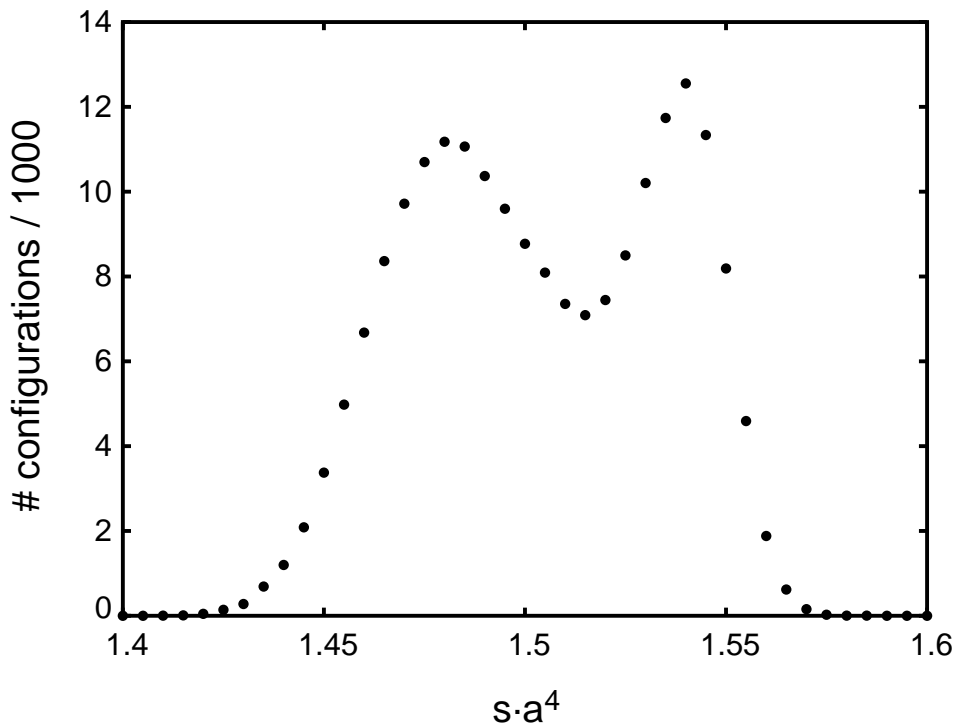


Figure 3: Distribution of the action density s at the deconfining phase transition, for a pure vortex world-surface curvature action with $c_1 = 0.4537$ and $c_2 = 0.5037$. The measurement was taken on a $26^3 \times 2$ lattice.

As a next step, in order to approach the condition (18), it is necessary to increase c_2 over c_1 . For example, the set of curvature coefficients $c_1 = 0.4537$, $c_2 = 0.5037$ yields $\sigma_2/\sigma_1 = 1.17$ while simultaneously realizing the deconfinement transition on a $N_t = 2$ lattice, cf. Fig. 3. Examining the trends, one notices an unexpected behavior: As one attempts to modify the parameters to approach the condition (18), the first-order character of the phase transition is weakened. In fact, when (18) is finally satisfied in

this way, the action discontinuity at the phase transition has either become undetectably small or has disappeared entirely, rendering the deconfinement transition second order. To be specific, the author used string tension measurements on $N_t = 2$ lattices in addition to the zero-temperature measurements to locate the set of parameters $c_1 = 0.428$, $c_2 = 0.540$ which yields (18) as well as realizing the deconfinement transition at $N_t = 2$; then, a careful scan of c_1 in steps of 0.0001 around $c_1 = 0.428$ was performed (with $c_2 = c_1 + 0.112$ in each case), generating the action density distributions on large ($30^3 \times 2$) lattices. No evidence of first order behavior was found.

This qualitative behavior can be confirmed for other N_t . For $N_t = 1$, the deconfinement transition occurs at $c_1 = 0.253$, $c_2 = 0.353$ (with (18) also satisfied). Likewise, for $N_t = 3$, the transition occurs at $c_1 = 0.538$, $c_2 = 0.571$. In both cases, a careful scan in c_1 , as above, with $c_2 - c_1$ fixed, reveals no first-order behavior. By extension, also the phase transition at the interpolated set of parameters realizing the remaining condition (17) is not discernibly first order.

Thus, it must be concluded that the conditions (18) and (24) are incompatible as long as one restricts oneself to a pure world-surface curvature action. One can realize either the one or the other condition, but one cannot model both simultaneously.

Before seeking to remedy this by generalizing the action, it is nevertheless useful to record here, for later reference, the simplified model which results if one disregards the first-order character of the deconfinement phase transition, i.e., if one disregards (24), and uses a pure world-surface curvature action. The two curvature coefficients c_1 and c_2 are then fixed using only the two conditions (18) and (17) as follows. Table 1 summarizes again the pairs of curvature coefficients at which the deconfinement transition occurs for $N_t = 1, 2, 3$ while (18) is simultaneously satisfied.

	c_1	c_2	$T_c/\sqrt{\sigma_1}$
$N_t = 1$	0.253	0.353	0.85
$N_t = 2$	0.428	0.540	0.60
$N_t = 3$	0.538	0.571	0.50

Table 1: Sets of coupling constants realizing the deconfinement temperature as well as satisfying (18). Condition (17) is then satisfied by interpolating the parameters using the data in the final column.

The table furthermore records the ratio $T_c/\sqrt{\sigma_1}$ corresponding to each parameter set. To obtain the physical point, one constructs the quadratic interpolations of the curvature coefficients c_1 and c_2 as functions of $T_c/\sqrt{\sigma_1}$. Setting $T_c/\sqrt{\sigma_1}$ equal to its physical value, cf. (17), yields the “physical” set of curvature coefficients

$$c_1 = 0.41 \qquad c_2 = 0.53 . \qquad (25)$$

Since the ratio σ_2/σ_1 satisfies (18) for all parameter sets used in the interpolation, it is expected to satisfy that condition also at the physical point (25). On the other hand,

this quantity can also be evaluated directly at the physical point, providing a cross-check of the interpolation procedure. Measuring σ_2/σ_1 directly for the parameters (25) yields the value $\sigma_2/\sigma_1 = 1.37$, deviating only slightly from (18). This is adequate for the present simplified model, which is only constructed here for comparison purposes. Indeed, in the comprehensive model discussed further below, the analogous cross-check of the interpolation procedure yields complete agreement with (18) at the physical point.

Having determined the “most physical” set of curvature coefficients (25) within this restricted model framework, one can predict the behavior of the string tensions at finite temperatures. The most significant quantitative prediction which is accessible in this way is the behavior of the *spatial* quark and diquark string tensions, σ_1^S and σ_2^S , in the deconfined phase. For the parameter set (25), the deconfined phase is realized for $N_t = 1$, which corresponds to the temperature⁹ $T = 1.9 T_c$, as one can infer by measuring the zero-temperature quark string tension σ_1 in lattice units and using (17). At this temperature, one obtains

$$\sigma_1^S(T = 1.9 T_c)/\sigma_1(T = 0) = 1.61 \quad \sigma_2^S(T = 1.9 T_c)/\sigma_2(T = 0) = 1.46 . \quad (26)$$

Thus, the spatial diquark string tension rises less strongly in the deconfined phase than the spatial quark string tension; the ratio between the two at $T = 1.9 T_c$ is reduced to

$$\sigma_2^S(T = 1.9 T_c)/\sigma_1^S(T = 1.9 T_c) = 1.25 \quad (27)$$

compared to the zero-temperature value $\sigma_2/\sigma_1 = 1.36$.

5.2 Effect of world-surface area term

As a first attempt to generalize the action in order to obtain a more realistic phenomenology, the effect of the world-surface area term (13) was briefly explored. This type of term was already investigated within the $SU(2)$ and $SU(3)$ models [21, 24] and ultimately discarded, since it did not enhance the phenomenological flexibility of those models. In the $SU(4)$ model, it can be used to differentiate between the two types of vortices without abandoning $c_1 = c_2$. Thus, the condition $c_1 = c_2$ was maintained, and instead (13) with $A(0) = A(1) = 0$ but nonvanishing $A(2)$ was introduced in the hope of maintaining a discernible first-order deconfinement transition while approaching the condition (18).

As an example, using $A(2) = 0.130$, the set of curvature coefficients $c_1 = c_2 = 0.460$ yields $\sigma_2/\sigma_1 = 1.17$ while simultaneously realizing the deconfinement transition on a $N_t = 2$ lattice, cf. Fig. 4. The behavior is similar to the one observed above in the case of a pure curvature action; approaching condition (18) weakens the action density discontinuity at the phase transition. In fact, in the present case, the discontinuity is

⁹Note that string tensions at other temperatures above T_c are not directly accessible at (25), but can be obtained using interpolations of measurements at other parameter sets to the physical point (25), cf. [21]. This was not pursued further here.

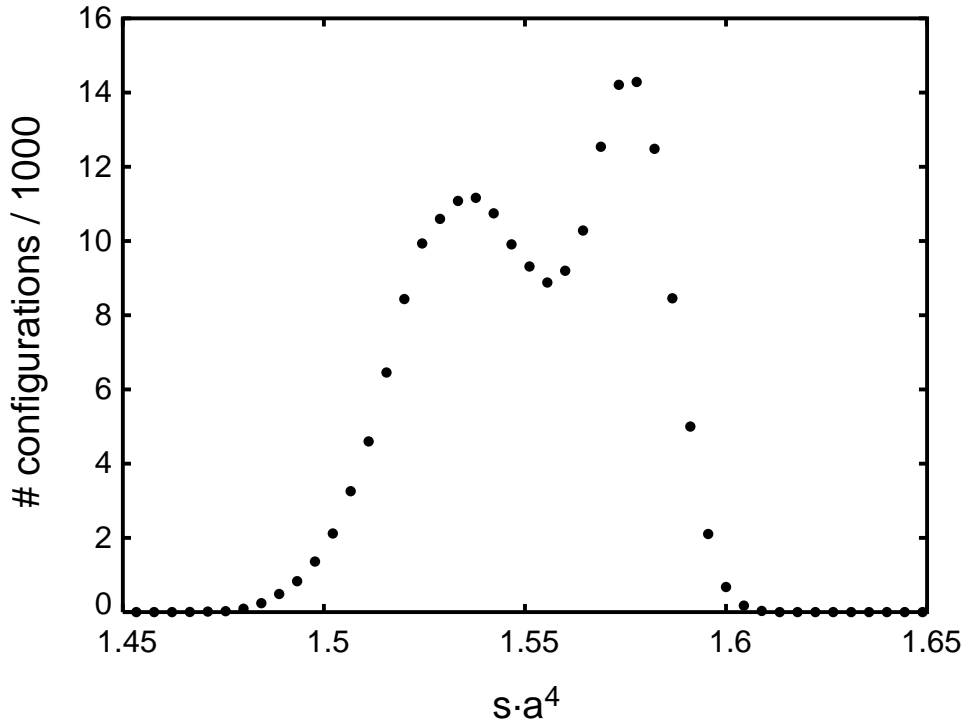


Figure 4: Distribution of the action density s at the deconfining phase transition, for an action containing a vortex world-surface curvature term with $c_1 = c_2 = 0.460$ and a world-surface area term with $A(2) = 0.130$. The measurement was taken on a $30^3 \times 2$ lattice.

even more strongly suppressed than in the analogous pure curvature case at the same ratio $\sigma_2/\sigma_1 = 1.17$. Thus, introducing the world-surface area term exacerbates the problem rather than alleviating it.

Increasing $A(2)$ further, when (18) is fully satisfied, the discontinuity indeed has disappeared again. When $A(2) = 0.300$, the deconfinement transition occurs at $c_1 = c_2 = 0.439$, and (18) simultaneously holds. The author again carried out a careful scan of $c_1 = c_2$ in steps of 0.0001 around this point and found no evidence of first order behavior.

5.3 Branching term

As has become clear from the preceding sections, a vortex model action based purely on the world-surface characteristics curvature and area is no longer phenomenologically viable in the $SU(4)$ case. This provides the motivation for introducing the new branching term (14) into the vortex model action. The reason for this particular choice lies in the following observation. Both the $SU(2)$ and the $SU(3)$ vortex models [21, 24] are

governed by the same type of action; nevertheless, the $SU(3)$ model exhibits a clear first-order deconfinement transition, whereas the $SU(2)$ model does not. The difference between the two models lies in the class of allowed vortex topologies; only the $SU(3)$ model provides for vortex branching. In view of this, it seems plausible to assume that facilitating vortex branching is conducive to a first-order deconfinement phase transition. Therefore, introducing a new action term encouraging vortex branching, such as (14), into the $SU(4)$ vortex model is expected to provide a viable mechanism for restoring phenomenologically correct behavior at the phase transition. This expectation is confirmed by the measurements discussed in the following.

The physical point of the model was determined in analogy to the procedure used in section 5.1. Properties of the deconfinement transition generally are not directly accessible for the physical set of coupling constants; instead, they are inferred by interpolation of phase transition data obtained at different N_t . Specifically, for $N_t = 1, 2, 3$ the parameter sets were determined which realize the deconfinement temperature while simultaneously satisfying both of the conditions (18) and (24). These parameter sets are listed in Table 2, and corresponding action density distributions illustrating the first-order behavior of the phase transitions are displayed in Figs. 5-7.

	c_1	c_2	b	$T_c/\sqrt{\sigma_1}$
$N_t = 1$	0.2785	0.4005	0.1403	0.90
$N_t = 2$	0.4558	0.7983	0.6950	0.61
$N_t = 3$	0.5925	0.7059	0.3800	0.50

Table 2: Sets of coupling constants realizing the deconfinement temperature as well as satisfying two of the three conditions defining the physical point, namely (18) and (24). The remaining condition (17) is subsequently satisfied by interpolating the parameters using the data in the final column.

The table furthermore records the ratio $T_c/\sqrt{\sigma_1}$ corresponding to each parameter set. To obtain the physical point, one constructs the quadratic interpolations of the coupling constants c_1 , c_2 and b as functions of $T_c/\sqrt{\sigma_1}$. Setting $T_c/\sqrt{\sigma_1}$ equal to its physical value, cf. (17), yields the physical point

$$c_1 = 0.45 \quad c_2 = 0.80 \quad b = 0.71 \quad (28)$$

As is evident from Table 2, the physical point is very near the parameters obtained for $N_t = 2$; the uncertainties inherent in the interpolation thus remain small. Since the conditions (18) and (24) were satisfied for all parameter sets used in the interpolation, they are expected to be satisfied at the the physical point (28) as well. In the case of (18), this can be cross-checked. Measuring σ_2/σ_1 directly at the physical point indeed yields agreement with (18). Of course, (24) cannot be cross-checked directly at the physical point.

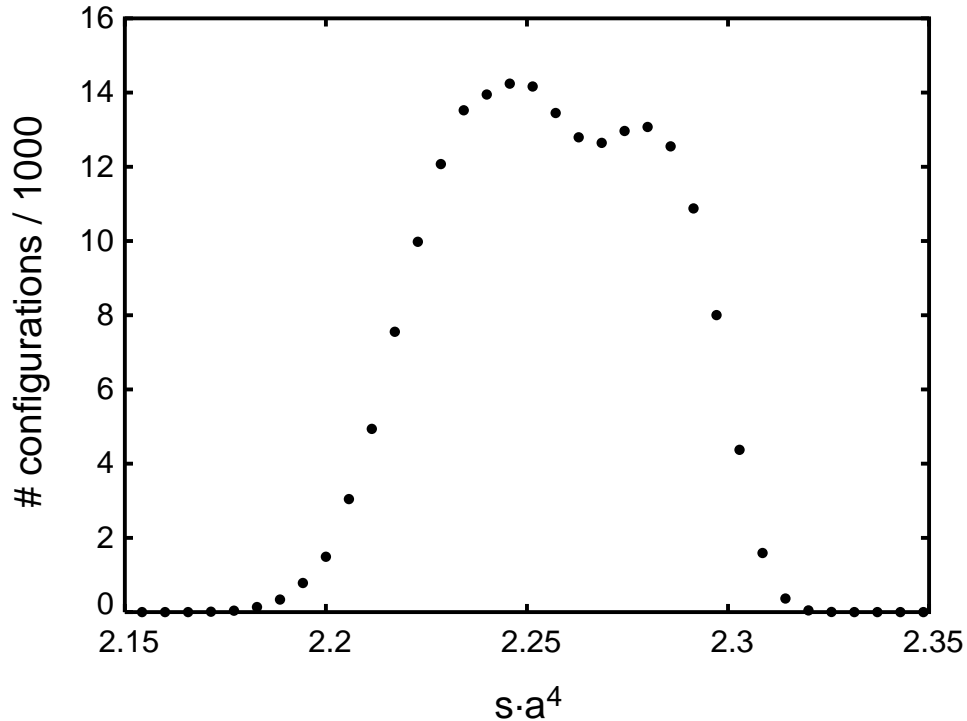


Figure 5: Distribution of the action density s at the deconfining phase transition, for an action containing a vortex world-surface curvature term with $c_1 = 0.2785$, $c_2 = 0.4005$ and a branching term with $b = 0.1403$. The measurement was taken on a $30^3 \times 1$ lattice. Taking the distance between the two maxima as a rough measure of the action density discontinuity Δs and supplementing this with a measurement of the zero-temperature quark string tension σ_1 in lattice units at the same set of coupling parameters, the condition (24) is satisfied by this first-order transition.

To appreciate the ultraviolet cutoff scale, it is useful to cast the lattice spacing a in physical units. Setting the zero-temperature quark string tension to $\sigma_1 = (440 \text{ MeV})^2$, and combining this with the measurement of that string tension in lattice units at the physical point, $\sigma_1 a^2 = 0.68$, yields

$$a = 0.37 \text{ fm} . \quad (29)$$

Within the framework of the random vortex world-surface model, this simultaneously characterizes the transverse thickness of the vortices, since it implements a minimal distance which parallel vortices must be apart in order to remain distinguishable. In the present $SU(4)$ case, this distance is slightly smaller than in the $SU(2)$ and $SU(3)$ cases, in which the minimal distance is 0.39 fm. As already noted further above, the fact that both of the two physically distinct types of vortices present in the $SU(4)$ model are

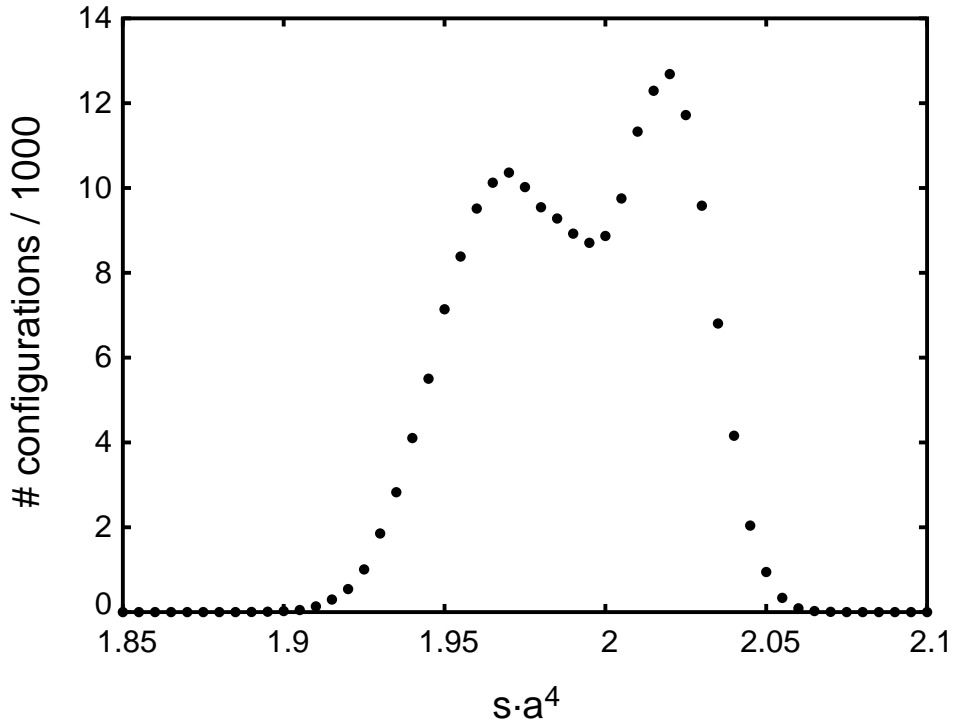


Figure 6: Distribution of the action density s at the deconfining phase transition, for an action containing a vortex world-surface curvature term with $c_1 = 0.4558$, $c_2 = 0.7983$ and a branching term with $b = 0.6950$. The measurement was taken on a $18^3 \times 2$ lattice. Taking the distance between the two maxima as a rough measure of the action density discontinuity Δs and supplementing this with a measurement of the zero-temperature quark string tension σ_1 in lattice units at the same set of coupling parameters, the condition (24) is satisfied by this first-order transition.

treated as having the same thickness is a model restriction due to the present hypercubic lattice formulation; in general, there is no physical reason forcing the two thicknesses to be the same. Note also that a decrease of the average vortex thickness as the number of colors is raised seems plausible in view of the qualitative picture discussed in section 2.4, cf. Fig. 1.

Having modeled the lattice Yang-Mills data presented in section 4, it is possible to predict string tensions at finite temperatures. In particular, the quantitative behavior of the spatial string tensions σ_1^S and σ_2^S in the deconfined phase can be accessed. At the physical point (28), a lattice with $N_t = 1$ realizes the temperature¹⁰ $T = 1.95 T_c$, and

¹⁰This temperature determination is minimally adjusted compared to the value quoted in the preliminary report [34] due to improved statistics in the calculation of the zero-temperature string tension.

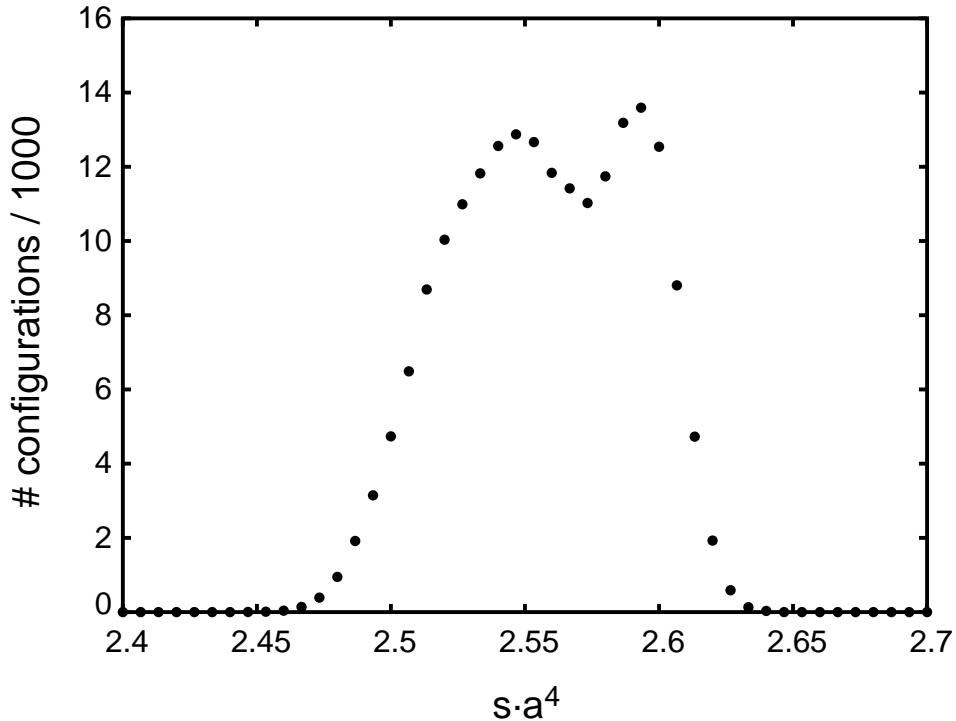


Figure 7: Distribution of the action density s at the deconfining phase transition, for an action containing a vortex world-surface curvature term with $c_1 = 0.5925$, $c_2 = 0.7059$ and a branching term with $b = 0.3800$. The measurement was taken on a $20^3 \times 3$ lattice. Taking the distance between the two maxima as a rough measure of the action density discontinuity Δs and supplementing this with a measurement of the zero-temperature quark string tension σ_1 in lattice units at the same set of coupling parameters, the condition (24) is satisfied by this first-order transition.

one obtains

$$\sigma_1^S(T = 1.95 T_c)/\sigma_1(T = 0) = 1.34 \quad \sigma_2^S(T = 1.95 T_c)/\sigma_2(T = 0) = 1.44 . \quad (30)$$

While both string tensions exhibit the characteristic rise with temperature in the deconfined phase, the behavior of σ_1^S in particular is quite different from the simplified model discussed in section 5.1. In contradistinction to that model, here, σ_1^S rises less strongly than σ_2^S , and the ratio of the spatial diquark string tension to the spatial quark string tension is enhanced at $T = 1.95 T_c$,

$$\sigma_2^S(T = 1.95 T_c)/\sigma_1^S(T = 1.95 T_c) = 1.46 \quad (31)$$

compared to the zero-temperature value $\sigma_2/\sigma_1 = 1.36$. This should be contrasted with the behavior in the aforementioned simplified model, where $\sigma_2^S(T = 1.9 T_c)/\sigma_1^S(T = 1.9 T_c) = 1.25$, cf. (27).

Furthermore, in the more recent survey of $SU(4)$ lattice Yang-Mills characteristics [33], which became available to the author after the bulk of the numerical work in the present investigation was completed, data for this string tension ratio are reported. According to these data, the ratio σ_2^S/σ_1^S remains near its zero-temperature value in the temperature regime considered here. Thus, while the comprehensive vortex model constructed in the present section adjusts the value of σ_2^S/σ_1^S in the correct direction compared to the simplified model of section 5.1, the adjustment overshoots the $SU(4)$ lattice Yang-Mills result considerably. The result (31) is almost as far above the lattice data as the corresponding result in the simplified model, (27), is below those data.

It should be noted that readjusting the present model to reproduce updated values from [33] for the observables discussed in section 4 would of course impact this comparison. On the other hand, regardless of the outcome of such an exercise, a further refinement of the $SU(4)$ vortex model action would presumably permit fitting also the finite-temperature spatial string tension ratio correctly, in addition to the observables of section 4. For instance, one could contemplate using a coupling constant $c_{12} \neq c_1 \cdot c_2$ in the curvature action (10); while this option was discarded above due to its physical similarity to the branching action (14), it is not precisely the same and thus may allow for some additional quantitative tuning. Another possible source of discrepancies between the model constructed here and $SU(4)$ Yang-Mills theory is the artificial restriction to a common thickness for both types of vortices present for $SU(4)$ color. Refinements along these lines will not be considered further here. If anything, such an endeavor would only further reinforce the conclusions drawn in the next, concluding, section below.

6 Conclusions

The goal of this investigation was to construct a random vortex world-surface model for $SU(4)$ Yang-Mills theory, particularly with a view towards the question whether infrared $SU(4)$ Yang-Mills phenomenology forces one to abandon the dynamical concept employed in the $SU(2)$ and $SU(3)$ cases, which is based purely on vortex world-surface characteristics. General arguments, put forward in [30] and reviewed in section 2, suggest that a shift away from this type of dynamics occurs as the number of colors is raised, with additional color structures present on the vortex world-surfaces attaining their own dynamical significance and influencing the vortex ensemble.

The modeling effort carried out in this work supports these arguments. It proved impossible to construct a vortex model which reproduces the main infrared characteristics of $SU(4)$ Yang-Mills theory based purely on a vortex world-surface curvature action. Instead, an explicit weighting of vortex branchings, which, depending on the color description, are associated with magnetic monopoles or nexi, turned out to furnish the additional flexibility needed to match $SU(4)$ Yang-Mills theory.

The need to introduce new action terms of course impacts the predictive capability of the model. Indeed, the effortless predictivity of the $SU(2)$ and $SU(3)$ models, in

which merely one dimensionless curvature coefficient needed to be adjusted, is lost in the $SU(4)$ case. Three dimensionless parameters were necessary to obtain a sufficiently flexible model. After having determined these parameters, the behavior of the spatial string tensions at high temperatures was predicted and compared to newer lattice Yang-Mills data which became available subsequently. It should be noted that the predictions are obtained at the ultraviolet limit of validity of the vortex model, and thus can be expected to be more prone to error than observables at lower temperatures; nevertheless, the discrepancy in the ratio of the spatial diquark to the spatial quark string tension at $T \approx 2T_c$, amounting to about 7%, seems significant. Aside from the possibility that this comparison may improve after readjusting the present vortex model to reproduce updated values from [33] for the observables discussed in section 4, further model refinements, as suggested at the end of section 5.3, would presumably permit closing this gap in any case. However, this would merely exacerbate the loss of predictive capability, already noted above, compared with the $SU(2)$ and $SU(3)$ vortex models.

In view of this, it does not seem attractive to pursue the construction of a yet more detailed $SU(4)$ vortex model. Indeed, the main question which this investigation aimed to address can be answered in the affirmative already at the present stage, as discussed above: As the number of colors is raised beyond $N = 3$ in $SU(N)$ Yang-Mills theory, the corresponding infrared effective vortex description cannot continue to rely on dynamics based purely on vortex world-surface characteristics. Solid evidence for this emerges in the $N = 4$ case studied in this work. To restore the correct $SU(4)$ Yang-Mills phenomenology at the deconfining phase transition, a generalization of the vortex model action was necessary, and an explicit dependence of the dynamics on vortex branching characteristics proved sufficient to achieve that goal.

Acknowledgments

Fruitful discussions with M. Quandt and H. Reinhardt are acknowledged. This work was supported by the U.S. DOE under grant number DE-FG03-95ER40965.

References

- [1] G. 't Hooft, Nucl. Phys. **B138** (1978) 1.
- [2] Y. Aharonov, A. Casher and S. Yankielowicz, Nucl. Phys. **B146** (1978) 256.
- [3] J. M. Cornwall, Nucl. Phys. **B157** (1979) 392.
- [4] G. Mack, Phys. Rev. Lett. **45** (1980) 1378.
- [5] H. B. Nielsen and P. Olesen, Nucl. Phys. **B160** (1979) 380.
- [6] L. Del Debbio, M. Faber, J. Greensite and Š. Olejník, Phys. Rev. D **55** (1997) 2298.

- [7] L. Del Debbio, M. Faber, J. Giedt, J. Greensite and Š. Olejník, Phys. Rev. D **58** (1998) 094501.
- [8] J. Greensite, Prog. Part. Nucl. Phys. **51** (2003) 1.
- [9] T. G. Kovács and E. T. Tomboulis, Phys. Rev. D **57** (1998) 4054.
- [10] T. G. Kovács and E. T. Tomboulis, J. Math. Phys. **40** (1999) 4677.
- [11] T. G. Kovács and E. T. Tomboulis, Phys. Rev. Lett. **85** (2000) 704.
- [12] J. M. Cornwall, Phys. Rev. D **58** (1998) 105028.
- [13] J. M. Cornwall, Phys. Rev. D **61** (2000) 085012.
- [14] J. M. Cornwall, Phys. Rev. D **65** (2002) 085045.
- [15] M. Engelhardt, K. Langfeld, H. Reinhardt and O. Tennert, Phys. Lett. **B431** (1998) 141.
- [16] M. Engelhardt, K. Langfeld, H. Reinhardt and O. Tennert, Phys. Rev. D **61** (2000) 054504.
- [17] R. Bertle, M. Engelhardt and M. Faber, Phys. Rev. D **64** (2001) 074504.
- [18] P. de Forcrand and M. D’Elia, Phys. Rev. Lett. **82** (1999) 4582.
- [19] C. Alexandrou, M. D’Elia and P. de Forcrand, Nucl. Phys. Proc. Suppl. **83** (2000) 437.
- [20] P. de Forcrand and L. von Smekal, Phys. Rev. D **66** (2002) 011504.
- [21] M. Engelhardt and H. Reinhardt, Nucl. Phys. **B585** (2000) 591.
- [22] M. Engelhardt, Nucl. Phys. **B585** (2000) 614.
- [23] M. Engelhardt, Nucl. Phys. **B638** (2002) 81.
- [24] M. Engelhardt, M. Quandt and H. Reinhardt, Nucl. Phys. **B685** (2004) 227.
- [25] M. Engelhardt, Phys. Rev. D **70** (2004) 074004.
- [26] M. Quandt, H. Reinhardt and M. Engelhardt, Phys. Rev. D **71** (2005) 054026.
- [27] M. Quandt, H. Reinhardt and M. Engelhardt, PoS **LAT2005** (2005) 320.
- [28] M. Engelhardt and H. Reinhardt, Nucl. Phys. **B567** (2000) 249.
- [29] F. Bruckmann and M. Engelhardt, Phys. Rev. D **68** (2003) 105011.
- [30] J. Greensite and Š. Olejník, JHEP **0209** (2002) 039.
- [31] B. Lucini, M. Teper and U. Wenger, JHEP **0401** (2004) 061.
- [32] B. Lucini, M. Teper and U. Wenger, JHEP **0406** (2004) 012.
- [33] B. Lucini, M. Teper and U. Wenger, JHEP **0502** (2005) 033.
- [34] M. Engelhardt, PoS **LAT2005** (2005) 319.